EDGE ARTICLE
Shun Dekura, Hatsumi Mori *et al.*
Isotropic proton conduction in an anisotropic crystal:
the role of molecular rotational dynamics in imidazolium
dihydrogen phosphate

Isotropic proton conduction in an anisotropic crystal: the role of molecular rotational dynamics in imidazolium dihydrogen phosphate

Shun Dekura, [iD] *[ab] Motohiro Mizuno [iD] [cde] and Hatsumi Mori [iD] *[a]

Understanding the intrinsic anhydrous proton conductivity and conduction mechanisms of solid electrolytes is of fundamental academic importance for their application in next-generation, non-humidified fuel cells. In this study, we investigated the anhydrous proton conductivity of single crystals of imidazolium dihydrogen phosphate (**1**), a material in which rotational motion of both the acid and base components is expected to contribute to the conduction mechanism. By controlling the crystallization conditions, we successfully and selectively prepared two polymorphs: a thermodynamically stable, non-centrosymmetric orthorhombic form (**1A**) and a metastable, centrosymmetric monoclinic form (**1B**). Single-crystal X-ray diffraction analysis of the stable phase **1A** revealed an anisotropic crystal structure with one-dimensional hydrogen-bonding phosphate chains connected with N–H···O hydrogen bonds with imidazolium. Nevertheless, the intrinsic anhydrous proton conductivity, evaluated using single crystals, exhibited nearly isotropic behavior with minimal directional dependence. Solid-state ^2H NMR measurements revealed that the imidazolium cations undergo active libration motion even at room temperature. We conclude that the dynamic motion of the imidazolium cations, in addition to the known rotational motion of the $H_2PO_4^-$ anions, effectively connects the proton conduction pathways, resulting in isotropic conductivity despite the anisotropic hydrogen-bond network. These findings demonstrate that the cooperative rotational dynamics of both acid and base components is a valid strategy for designing high-performance anhydrous proton-conducting materials.

Introduction

Anhydrous organic proton conductors are attracting attention not only for their application as solid electrolytes in next-generation fuel cells that do not require humidification but also from a fundamental perspective, as they can realize intrinsic proton conduction phenomena free from extrinsic factors. Although high conductivity has been reported in systems where acids or bases are doped into porous materials like organic polymers, MOFs, and COFs,[1–3] a comprehensive understanding of the anhydrous proton conduction mechanism remains undeveloped, and a rational design principle for

achieving high proton conductivity has not yet been established.

To elucidate the mechanism of anhydrous proton conduction, it is essential to clarify the structure–property relationships based on clear structural information and precise physical property measurements using single-crystalline samples, which are free from the influence of defects such as grain boundaries. From this viewpoint, molecular single-crystalline materials provide an ideal platform. In fact, several groups have recently reported studies on structure–property correlations using such molecular single crystals.[4–12] For elucidation of the intrinsic anhydrous proton conductivity and the conduction mechanism, we have focused on acid–base-type molecular co-crystals, which allow for versatile material design through the combination of constituent molecules and are advantageous for forming extended hydrogen-bond networks. In previous work on a series of imidazolium dicarboxylate single crystals, it was revealed that, in addition to static factors such as (1) hydrogen-bond network structures and (2) the difference in acidity between constituent molecules (ΔpK_a), (3) molecular rotational motion in crystals is a crucial factor for achieving high anhydrous proton conductivity.[8,9,11] These three factors correspond to the essential factors for the Grotthuss mechanism proposed for hydrous systems:[13] (1) the

[a]The Institute for Solid State Physics, The University of Tokyo, Chiba 277-8581, Japan. E-mail: hmori@issp.u-tokyo.ac.jp

[b]Institute of Multidisciplinary Research for Advanced Materials (IMRAM), Tohoku University, 2-1-1 Katahira, Aoba-ku, Sendai 980-8577, Japan. E-mail: s.dekura@tohoku.ac.jp

[c]Graduate School of Natural Science and Technology, Kanazawa University, Kakuma-machi, Kanazawa, Ishikawa 920-1192, Japan

[d]NanoMaterials Research Institute, Kanazawa University, Kakuma-machi, Kanazawa, Ishikawa 920-1192, Japan

[e]Institute for Frontier Science Initiative, Kanazawa University, Kakuma-machi, Kanazawa, Ishikawa 920-1192, Japan

construction of proton conduction pathways, (2) inter-molecular proton transfer through hydrogen bonds, and (3) "intra-"molecular proton transfer where protons move from one side of a molecule to the other, respectively. This indicates that anhydrous proton conduction can be understood based on Grotthuss-like mechanistic picture.

Among these factors, the effect of molecular motion in crystals, which is responsible for intra-molecular proton transfer, on anhydrous proton conductivity remains largely unexplored. In ionic conductors such as lithium ion conductors, a "paddle-wheel mechanism" has been reported, where high ionic conduction is accompanied with the rotational dynamics of the counter anions.[14] However, a recent simulation study reported the opposite results.[15] Moreover, unlike other ionic conduction with such a paddle-wheel mechanism, where the ions can solely conduct throughout the crystal and are thought to be significantly decoupled from the molecular rotational dynamics, protons are bound to hydrogen bonds, and thus proton conduction is strongly coupled with the rotational dynamics, which is considered to be one of the essential processes for proton conduction.[9] Previous studies have reported that imidazole (**Im**) or its analogues doped or incorporated into MOFs or polymers exhibit rotational motion on heating, which is accompanied by an improvement in anhydrous proton conductivity.[16–23] Furthermore, other studies on protic organic ionic plastic crystals (POIPCs) have reported the relation between the emergence of a plastic crystalline phase and proton conduction.[24,25] However, such systems with unclear structural information and/or chemical compositions and serious contribution of defects did not allow for the evaluation of the intrinsic anhydrous proton conductivity. Therefore, both the materials developments of anhydrous proton conductors with expected significant molecular rotational motions in crystals and the understanding of their intrinsic proton conductivity are highly demanded.

We have focused on the combination of the phosphate anion ($H_2PO_4^-$) known to induce superprotonic phase transitions *via* its vigorous rotational motion in inorganic solid acids,[26,27] and the imidazolium cation (**ImH$^+$**) with reported librational motion in crystals, to develop anhydrous proton-conducting molecular crystals with rotational motions of both acid and base components. In a previous study, we successfully prepared high-quality single crystals of phosphoric acid imidazolium dihydrogen phosphate, a co-crystal with a 2 : 1 ratio of phosphoric acid to **Im**, and revealed that it exhibits high and isotropic anhydrous proton conductivity over 10^{-3} S cm^{-1} despite its anisotropic crystal structure.[12] Significant three-dimensional (3D) rotational motion of **ImH$^+$** was observed; however, the anhydrous proton conduction was predominantly carried by the 3D hydrogen-bond network of phosphoric acid, with **ImH$^+$** playing a minor role in enhancing conductivity.

In this study, we prepared single crystals of imidazolium dihydrogen phosphate (=**1**; Fig. 1a), a 1 : 1 co-crystal of phosphoric acid and **Im**, and evaluated its anhydrous proton conductivity along each crystallographic axis. **1** was obtained as two different polymorphs (**1A** and **1B**) depending on the crystallization conditions. The thermodynamically stable form **1A**

possesses an anisotropic molecular arrangement containing both the proton conduction pathways based on $H_2PO_4^-$ alone and the pathways intervened by **ImH$^+$**. However, its single-crystal proton conductivity showed small anisotropy, reaching to about 10^{-5} S cm^{-1} at approximately 370 K in all crystallographic directions. Solid-state ^2H NMR measurements using deuterated sample revealed that **ImH$^+$** exhibits large librational motion in the **1A** crystals; this molecular motion, coupled to the known $H_2PO_4^-$ rotational motions, significantly contributes to the low-anisotropy conductivity of **1A**.

Results and discussion

Crystal structures of the polymorphs of 1

Two polymorphs of **1** have been reported in previous studies despite similar crystallization methods.[28–30] In this work, we successfully prepared these two polymorphs selectively by controlling the molar ratio of the starting materials. Recrystallization of a crude crystals, obtained by using **Im** and H_3PO_4 in a 1 : 1 molar ratio, from a methanol solution by vapor diffusion of acetone as a poor solvent consistently yielded high-quality, colorless rod-shaped single crystals (Fig. S1). In contrast, changing the starting molar ratio to **Im** : H_3PO_4 = 2 : 1 yielded colorless block-shaped single crystals (see the SI for details). Single-crystal X-ray structural analysis revealed that both were 1 : 1 co-crystals of **Im** : H_3PO_4, **1**. The former rod-shaped crystals were a polymorph with a polar orthorhombic $Pna2_1$ structure (= **1A**), while the latter block-shaped crystals were a polymorph with a non-polar monoclinic $P2_1/n$ structure (= **1B**). Thus, we succeeded in selectively preparing two different polymorphs solely by changing the starting molar ratio of the crude crystals. Melting point measurements showed that both **1A** and **1B** had the same melting points of 395–397 K. Both exhibited weak deliquescence; however, while **1A** maintained its crystal shape and single-crystal quality even after being exposed to the atmosphere for at least about a week, **1B** tended to become opaque overnight, suggesting it is less stable than **1A**.

The crystal structure of **1A** at room temperature is shown in Fig. 1 (see also Table S1). As mentioned above, **1A** crystallizes in a polar orthorhombic $Pna2_1$ space group, with one molecule each of **ImH$^+$** and $H_2PO_4^-$ as the crystallographically independent unit. The unit cell contains 4 pairs of **ImH$^+$** and $H_2PO_4^-$ (Z = 4). In the crystal structure, $H_2PO_4^-$ anions form one-dimensional (1D) hydrogen-bonded $[H_2PO_4^-]_\infty$ chains along the c axis *via* O–H···O hydrogen bonds ($d_{O-H···O}$ = 2.548(3), 2.588(2) Å). These chains adopt a ferroelectric polar arrangement with all the axial O–H groups pointing in the $-c$ direction (Fig. 1b and S3a–c). The O–H···O hydrogen-bond lengths over 2.5 Å and the clear single- and double-bond character in the P–O bond lengths (d_{P-O} = 1.505(1), 1.503(2), 1.561(2), 1.569(2) Å) suggest that the protons in the O–H···O hydrogen bonds are in double-well potentials. Furthermore, these $[H_2PO_4^-]_\infty$ chains are connected in the ab plane by **ImH$^+$** cations through N–H···O hydrogen bonds ($d_{N-H···O}$ = 2.644(2), 2.708(2) Å), resulting in the formation of a 3D hydrogen-bond network (Fig. 1c and d).

On the other hand, **1B** possesses a hydrogen-bond network structure significantly different from that of **1A** (Fig. S2, S3d–f
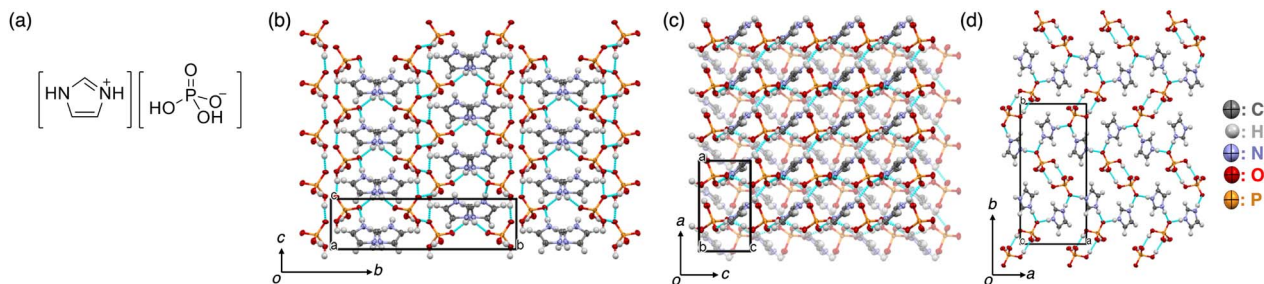
Fig. 1 (a) The chemical structure of **1**. (b)–(d) The crystal structure of the polymorph **1A** viewed along the (b) *a*, (c) *b*, and (d) *c* axes (C: gray, H: white, N: purple, O: red, P: orange). The light–blue dashed lines indicate the hydrogen bonds.

and Table S1). **1B** crystallizes in a non-polar monoclinic $P2_1/n$ space group, with two molecules each of **ImH$^+$** and $H_2PO_4^-$ as the crystallographically independent units. The unit cell contains 8 pairs of **ImH$^+$** and $H_2PO_4^-$ ($Z = 8$), and in the crystal structure, the $H_2PO_4^-$ anions form a 3D hydrogen-bond network *via* O–H⋯O hydrogen bonds ($d_{O-H\cdots O}$ = 2.561(2), 2.578(2), 2.581(2), 2.588(2) Å; Fig. S3d–f). Similar to **1A**, the O–H⋯O bond lengths exceeding 2.5 Å and the clear single- and double-bond character in the P–O bonds (d_{P-O} = 1.506(1), 1.510(1), 1.559(1), 1.559(1) Å and d_{P-O} = 1.490(2), 1.503(1), 1.541(2), 1.552(2) Å for the two crystallographically independent $H_2PO_4^-$) suggest that the protons in the O–H⋯O hydrogen bonds reside in double-well potentials. The **ImH$^+$** cations are incorporated into the voids of the 3D $[H_2PO_4^-]_\infty$ network, forming N–H⋯O hydrogen bonds with the $[H_2PO_4^-]_\infty$ framework ($d_{N-H\cdots O}$ = 2.700(2), 2.707(2), 2.712(2), 2.727(2) Å).

Although both **1A** and **1B** form 3D hydrogen-bond networks, their topologies are markedly different; **1A** possesses 1D $[H_2PO_4^-]_\infty$ chains and **1B** possesses a 3D $[H_2PO_4^-]_\infty$ framework. The average hydrogen-bond distances for **1A** and **1B** are $d_{O-H\cdots O}$ = 2.553(4) and 2.576(4) Å, and $d_{N-H\cdots O}$ = 2.676(3) and 2.712(4) Å, respectively; hydrogen bonds are shorter on average in **1A**. The calculated densities of **1A** and **1B** are ρ_{calc} = 1.615 and 1.583 g cm^{-3}, respectively, with **1A** being denser reflecting the difference in hydrogen-bond lengths. Considering these structural parameters, **1A** is suggested to be the more enthalpically stable polymorph, while **1B** is a metastable structure that preferentially crystallizes kinetically under **Im**-excess conditions.

Relative stability of the polymorphs

The similar melting points and crystallization conditions for **1A** and **1B** suggest that their comparable structural stabilities. To investigate their relative stability, we performed PXRD measurements on a crude crystals synthesized at room temperature and in an ice bath (Fig. S4). The PXRD pattern of the crude crystals obtained at room temperature matched the simulated pattern for **1A**. In contrast, the PXRD pattern of a crude crystals prepared in an ice bath showed partial inclusion of peaks attributed to **1B** (asterisks in Fig. S4). These experimental results suggest that **1A** is the thermodynamically most stable phase, while **1B** is a kinetically obtained metastable structure.

To corroborate this result, we compared the total energies of **1A** and **1B** by DFT calculations including Grimme's D3 dispersion correction. The calculation revealed that the **1A** structure is more stable than the **1B** structure by 46.6 meV (4.50 kJ mol^{-1}) per (**ImH$^+$**)($H_2PO_4^-$) pair (Tables S2 and S3; see the Experimental section in SI for details). Based on this experimental and theoretical evidences, we concluded that **1A** is enthalpically more stable than **1B**, and **1B** is a kinetically obtained metastable structure.

Intrinsic anhydrous proton conductivity of 1A

Since the single crystals of the metastable **1B** of sufficient quality for precise physical property measurements could not be obtained because of its instability as observed behavior becoming opaque overnight, this study focused on evaluating the intrinsic anhydrous proton conductivity of the most stable polymorph **1A**. The crystal structure of **1A** features 1D $[H_2PO_4^-]_\infty$ chains extending along the *c* axis while **ImH$^+$** cations are interposed between the chains in the *ab* plane. This suggests that protons can conduct *via* $H_2PO_4^-$ anions alone along the *c* axis whereas the rotational motion of both **ImH$^+$** and $H_2PO_4^-$ is essential for conduction along the *a* and *b* axes, leading to an expectation of anisotropic conductivity. Accordingly, we evaluated the intrinsic proton conductivity under anhydrous conditions along each crystallographic axis using high-quality single crystals of **1A** by AC impedance spectroscopy (Fig. 2 and S5–S8). Previous studies mainly used polycrystalline powders, which yield complex impedance spectra affected by grain boundaries and defects and make it difficult to evaluate intrinsic conductivity.[2,8,10,31–33] In contrast, our single-crystal measurements allowed us to observe a perfect semicircular trace on the Nyquist plot (Fig. 2a). This indicates a Debye-type dielectric relaxation with a single relaxation time, showing that the observed dielectric response originates solely from the intrinsic proton transfer process within the crystal. The observation of a single plateau at each temperature in the Bode plot further supports that only a single dielectric relaxation process is being observed (Fig. 2b). For the *b*-axis measurement, as the temperature was increased from room temperature, distinct dielectric relaxation was observed above 324.3 K within the measurement range of the impedance analyzer. With further increasing temperature, the radius of the semicircle on the Nyquist plot decreased and the plateau on the Bode plot shifted to the high-
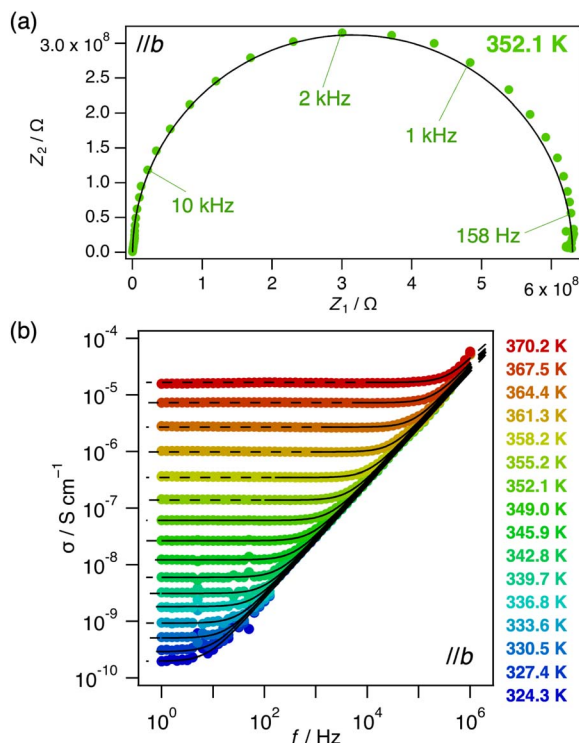
Fig. 2 (a) The Nyquist plot of the complex impedance of **1A** measured along the b axis at 352.1 K. (b) The Bode plot (σ *vs. f*) of **1A** measured along the b axis at various temperatures.
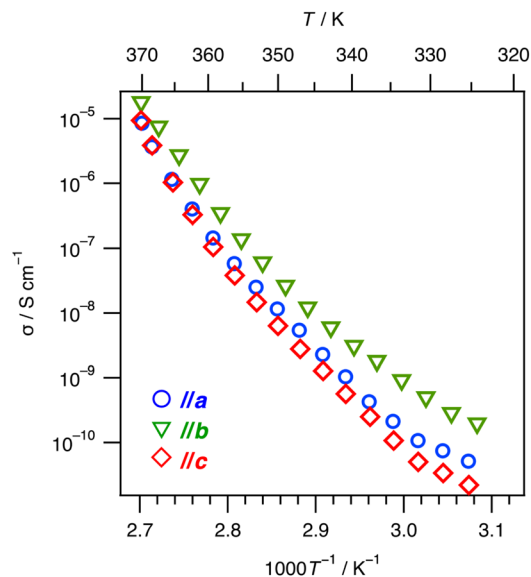

Fig. 3 Temperature dependence of the intrinsic anhydrous proton conductivity (σ) of the single-crystalline samples of **1A** (blue circles: along the a axis, green triangles: along the b axis, red diamonds: along the c axis).

conductivity side, demonstrating a thermally activated behavior of proton conductivity (Fig. S6). Measurements along the a and c axes also successfully observed a single dielectric relaxation process and thermally activated proton conduction, indicating that the intrinsic proton conductivity of **1A** was successfully evaluated (Fig. S5 and S7).

By fitting the frequency dependence of the complex impedance at each temperature for each crystallographic axis of **1A**, the DC conductivity, σ, was evaluated as the intrinsic anhydrous proton conductivity. Fig. 3 shows the temperature dependence of σ for each axis. Remarkably, despite the anisotropic molecular arrangement and hydrogen-bond network structure of **1A** (Fig. 1b–d), the anisotropy in proton conductivity was found to be quite small. The conductivity σ reached approximately 10^{-5} S cm^{-1} at about 370 K for all axes, with the conductivity along the b axis being the highest (Table 1). Furthermore, all axes exhibited non-Arrhenius behavior, with the Arrhenius plot deviating from a linear dependence, which suggests a complex conduction mechanism where molecular rotational dynamics is involved in the rate-determining step (Fig. S8).[9] The activation energy, E_a, was estimated for low- and high-temperature regions around *ca.* 340 K based on the Arrhenius plots. Apparent E_a increased with temperature, from 1.77–2.05 eV in the low-temperature region to 3.39–3.71 eV in the high-temperature region. The value of E_a was highest along the c axis parallel to the $[\mathrm{H_2PO_4}^-]_\infty$ chains, and lowest along the b axis, where **ImH$^+$** is interposed. While previous studies have reported an activation energy of about 1 eV for proton conduction in the

$[\mathrm{H_2PO_4}^-]_\infty$ network of phosphates,[4,5,26,34] **1A** shows a high E_a of about 2–4 eV, which is close to the values reported in previous studies of molecular **ImH$^+$** salt single crystals.[8,9,12] Therefore, it is expected that the molecular rotational motion of **ImH$^+$** is deeply involved in the conduction mechanism along all crystallographic directions of **1A**.

Proton conduction mechanism in 1A

To elucidate the origin of the observed nearly isotropic conductivity with the non-Arrhenius behavior, we evaluated the dynamics of **ImH$^+$** cations in the **1A** crystal by variable-temperature solid-state ^{2}H NMR measurements (Fig. 4). Solid-state ^{2}H NMR is a powerful technique enabling us to selectively evaluate dynamics in the kHz–MHz range, which is suitable for investigation of molecular motion in solids.[7,9,12] In this study, we prepared a deuterated powder sample of **1A** ($=$ **1A-d_3**) using deuterated **ImH$^+$** cations (**ImH$^+$-d_3**), where the C–H protons of **ImH$^+$** were H/D substituted (Fig. 4a). As shown in Fig. 4b, the obtained spectra from 303.4 K to 357.2 K showed characteristic Pake doublet patterns with a small sharp central peak. Although the intensity of the sharp peak increased with temperature, its spectral weight was only about 2.26% even at the highest temperature, suggesting it is an extrinsic behavior related to a small portion of sample damaged during flame sealing. The majority Pake doublet component showed peaks shifting toward the center and changes in spectral shape with increasing temperature, indicating that the rotational motion of the **ImH$^+$-d_3** cations was activated. The Pake doublet component at all temperatures was successfully reproduced by a spectral simulation assuming a three-site jump model of libration motion (Fig. 4a bottom, 4b and S9). The rate and the amplitude of the libration motion, k_{lib} and θ_{lib}, respectively,

**Table 1** Maximum anhydrous proton conductivity, σ_{max}, and the activation energy, E_a, of the single-crystalline samples of **1A** for each crystallographic direction

	//a	//b	//c
σ_{max} (S cm^{-1})	8.56×10^{-6} [370.1 K]	1.82×10^{-5} [370.2 K]	9.43×10^{-6} [370.2 K]
E_a (eV)	1.87(18) [325.4–340.9 K]	1.77(8) [324.3–339.7 K]	2.05(17) [325.3–340.8 K]
	3.40(13) [343.9–370.1 K]	3.39(9) [345.9–370.2 K]	3.71(15) [343.9–370.2 K]

estimated from the spectral simulation, increased from 4.0×10^3 Hz to 1.0×10^4 Hz and from 16° to 23°, respectively, as the temperature was raised from 303.4 K to 357.2 K (Fig. 4c). The activation energy based on the temperature dependence of k_{lib} is estimated to be 0.17(2) eV. Notably, it was revealed that even at room temperature (303.4 K), a large-amplitude libration motion of $\theta_{lib} = 16°$ occurs in **1A-d_3**. In previous studies on imidazolium succinate and glutarate with static dicarboxylate anions, a libration motion with θ_{lib} up to ~20° was rapidly excited by heating and only observed at high temperatures.[9,35] In contrast, in this study on **1A** as well as our previous work on a 1 : 2 ratio of **Im** : H$_3$PO$_4$,[12] where the molecular rotational dynamics of both acid and base is expected, significant molecular rotational dynamics was realized even at room temperature, suggesting that the adoption of the highly mobile H$_2$PO$_4^-$ as a counter-anion also activated the dynamics of **ImH$^+$**.

Based on the above results, we discuss the anhydrous proton conduction mechanism in **1A**. Anhydrous proton conduction in molecular crystals is considered based on (1) the construction of a hydrogen-bond network as a conduction pathway, (2) inter-molecular proton transfer via inter-molecular hydrogen bonds, and (3) intra-molecular proton transfer via molecular rotational motion.[9] Regarding (1) the conduction pathway, the crystal structure of **1A** has proton conduction pathways via hydrogen-bond networks in all the a, b, and c directions, which is consistent with the realization of proton conductivity in all directions. Focusing on (2) inter-molecular proton transfer, proton transfer along the c axis is achieved through the reaction $2H_2PO_4^- \leftrightarrow H_3PO_4 + HPO_4^{2-}$, while in the a direction, it is achieved through $H_2PO_4^- + \mathbf{ImH^+} \leftrightarrow H_3PO_4 + \mathbf{Im}$, and both occurring in the b direction. Given the pK_a values for H$_3$PO$_4$ (pK_{a1} = 2.15, pK_{a2} = 7.20) and **ImH$^+$** (pK_{aH}^+ = 6.99), the pK_a differences (ΔpK_a) for $H_2PO_4^-$–$H_2PO_4^-$ inter-molecular proton transfer (pK_{a2} − pK_{a1} = 5.05) and $H_2PO_4^-$–**ImH$^+$** transfer (pK_{aH}^+ − pK_{a1} = 4.84) are both large, suggesting high barriers for inter-molecular proton transfer in all directions. The fact that the maximum conductivity σ_{max} of **1A** remains at about 10^{-5} S cm^{-1} in all directions is likely due in part to this large barrier for inter-molecular proton transfer. However, considering that the proton transfer barrier is larger between $H_2PO_4^-$–$H_2PO_4^-$ than between $H_2PO_4^-$–**ImH$^+$**, the order of inter-molecular proton transfer barriers is //a > //b > //c, which is inconsistent with the order of σ (Fig. 3). The observation of non-Arrhenius behavior and the high E_a also suggest that (3) intra-molecular proton transfer via molecular rotational motions, rather than (2) inter-molecular proton transfer process, contributes significantly to the rate-determining step of proton conduction in **1A**.
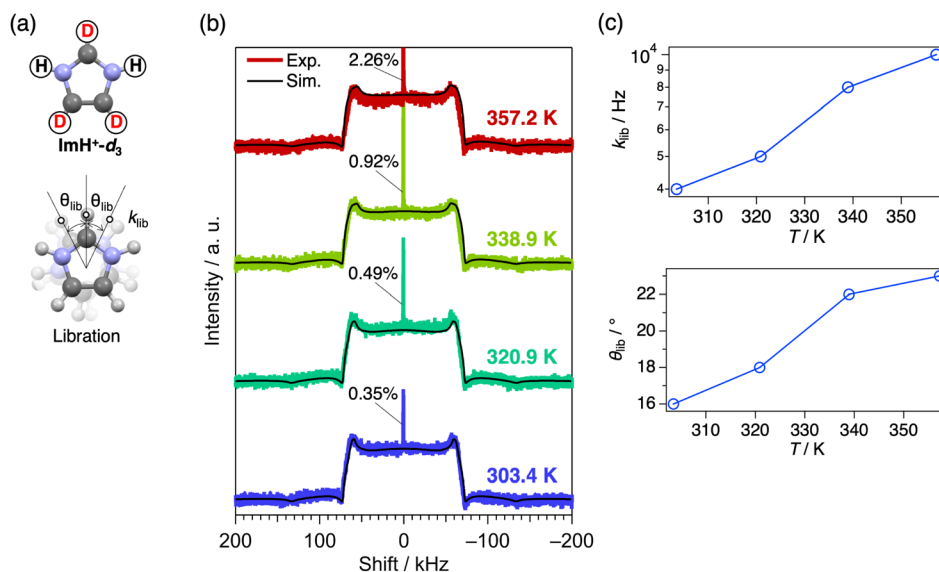
Fig. 4 (a) (Top) Positions of the substituted deuterium in **ImH$^+$-d_3**, and (bottom) schematics of the model assumed for the spectral simulations. The k_{lib} and θ_{lib} indicate the frequency of the libration and the libration angle, respectively. (b) Variable-temperature solid-state ^{2}H NMR spectra of **1A** (colored solid lines: experimental spectra, black solid lines: simulated spectra). (c) Temperature dependences of the parameters estimated from the spectral simulations: (top) the frequency of libration motion k_{lib}; (bottom) libration angle θ_{lib}. See also the SI for details.

According to previous studies on molecular phosphate and imidazolium salts, proton conduction *via* $H_2PO_4^-$ molecular rotation has an E_a of ~1 eV,[4,5,26,34] while conduction involving **ImH**$^+$ molecular rotational dynamics tends to have a higher E_a of > *ca.* 2 eV.[9,11,12] This suggests that the proton conduction mechanism in **1A** involves the molecular rotational motion of **ImH**$^+$ in all crystallographic directions. Indeed, solid-state ^2H NMR measurements using a deuterated sample observed that **ImH**$^+$ in the **1A** crystal exhibits large libration motion (Fig. 4). However, there is a notable difference between the two time-scales: the hopping frequency estimated from the impedance spectra is 10^1–10^6 Hz, whereas the libration rate observed by NMR is 10^3–10^4 Hz. This suggests that while the dynamics observed by NMR is related to the emergence of isotropic conductivity, it is not the specific dynamics involved in the rate-determining steps of the proton conduction. Note that the realization of molecular rotational dynamics is not trivial for the closely packed hydrogen-bonded molecular crystals like the salt **1A**. Therefore, the observed molecular rotational dynamics is strongly correlated to the isotropic conductivity in the anisotropic structure; the libration motion of **ImH**$^+$ related to intramolecular proton transfer is thermally excited, promoting proton conduction in the *a* and *b* directions. On the other hand, as mentioned above, a conduction pathway *via* **ImH**$^+$ is unlikely in the *c* direction, suggesting that **ImH**$^+$ cations are indirectly involved in anhydrous proton conduction along the *c* axis. In the crystal structure of **1A**, the $H_2PO_4^-$ anion forms hydrogen bonds with two **ImH**$^+$ cations; $H_2PO_4^-$ anion must break these hydrogen bonds for its own rotational motion. As the dynamics of **ImH**$^+$ being excited with temperature, these N–H⋯O hydrogen bonds between $H_2PO_4^-$ and **ImH**$^+$ become easier to break, which in turn facilitates the rotational motion of the $H_2PO_4^-$ anions, consequently promoting proton conduction. In other words, the anhydrous proton conduction in **1A** is governed by the rotational motion of both $H_2PO_4^-$ and **ImH**$^+$. In particular, the rotational motion of **ImH**$^+$ is deeply involved in the rate-determining step, dynamically linking the multiple conduction pathways present in the anisotropic crystal structure, thereby realizing nearly isotropic proton conductivity.

Conclusions

In this study, we prepared single crystals of imidazolium dihydrogen phosphate (= **1**), a 1 : 1 co-crystal of **Im** and H_3PO_4, successfully prepared its two polymorphs **1A** and **1B**, and elucidated their relative stability. The thermodynamically stable phase, **1A**, possesses an anisotropic hydrogen-bond network structure with 1D phosphate anion chains, yet the observed intrinsic anhydrous proton conductivity was surprisingly isotropic. Solid-state ^2H NMR measurements revealed that **ImH**$^+$ in the crystal undergoes active libration motion from low temperatures, suggesting that this molecular motion is deeply related to realization of the isotropic proton conduction. Taking into account the well-studied molecular rotational motion of $H_2PO_4^-$ anions from previous studies, it is concluded that the anhydrous proton conduction mechanism in **1A** is governed by the cooperative rotational motion of both the $H_2PO_4^-$ anions

and the **ImH**$^+$ cations. In particular, the dynamics of the **ImH**$^+$ cations in the crystal are thought to functionally activate the multiple conduction pathways present in the anisotropic hydrogen-bond network, realizing macroscopic isotropy in conductivity. To obtain a more direct picture of the dynamics involved in the rate-determining steps for proton conduction, further investigation such as quasi-elastic neutron scattering experiments or advanced molecular dynamics simulations are necessary. The findings of this research show that the realization and control of the molecular rotational dynamics of both acid and base components is an effective strategy in the design of high-performance anhydrous proton-conducting materials.

Finally, it is worth noting that even single-crystalline samples can contain point defects (*e.g.*, proton defects). Clarifying their effects on proton conductivity will be a crucial direction for future studies.

Author contributions

Conflicts of interest

There are no conflicts to declare.

Data availability

CCDC 2476711 and 2476720 contain the supplementary crystallographic data for this paper.[36a,b]

Supplementary information: Experimental details, single-crystal X-ray structural analyses, relative stability by DFT calculations, AC impedance spectroscopy, solid-sate ^2H NMR. See DOI: **https://doi.org/10.1039/d5sc05839b**.

Acknowledgements

References

1 R. Sahoo, S. Mondal, S. C. Pal, D. Mukherjee and M. C. Das, *Adv. Energy Mater.*, 2021, **11**, 2102300.

2 D. Mukherjee, A. Saha, S. Moni, D. Volkmer and M. C. Das, *J. Am. Chem. Soc.*, 2025, **147**, 5515–5553.

3 C. Pawlaczyk, A. Pawłowski, M. Połomska, K. Pogorzelec-Glaser, B. Hilczer, A. Pietraszko, E. Markiewicz, P. Ławniczak and L. Szcześniak, *Phase Transitions*, 2010, **83**, 854–867.

4 Y. Yoshii, N. Hoshino, T. Takeda and T. Akutagawa, *J. Phys. Chem. C*, 2015, **119**, 20845–20854.

5 G. Yuan, T. Takeda, N. Hoshino and T. Akutagawa, *J. Phys. Chem. C*, 2020, **124**, 1861–1871.

6 M. Tadokoro, M. Itoh, R. Nishimura, K. Sekiguchi, N. Hoshino, H. Kamebuchi, J. Miyazaki, F. Kobayashi, M. Mizuno and T. Akutagawa, *Chem.–Eur. J.*, 2022, **28**, e202201397.

7 C. Sato, S. Dekura, H. Sato, K. Sambe, T. Takeda, T. Kurihara, M. Mizuno, T. Taniguchi, J. Wu, T. Nakamura and T. Akutagawa, *J. Am. Chem. Soc.*, 2024, **146**, 22699–22710.

8 Y. Sunairi, A. Ueda, J. Yoshida, K. Suzuki and H. Mori, *J. Phys. Chem. C*, 2018, **122**, 11623–11632.

9 Y. Sunairi, S. Dekura, A. Ueda, T. Ida, M. Mizuno and H. Mori, *J. Phys. Soc. Jpn.*, 2020, **89**, 051008.

10 S. Dekura, Y. Sunairi, K. Okamoto, F. Takeiri, G. Kobayashi, Y. Hori, Y. Shigeta and H. Mori, *Solid State Ionics*, 2021, **372**, 115775.

11 Y. Hori, S. Dekura, Y. Sunairi, T. Ida, M. Mizuno, H. Mori and Y. Shigeta, *J. Phys. Chem. Lett.*, 2021, **12**, 5390–5394.

12 S. Dekura, M. Mizuno and H. Mori, *Angew. Chem., Int. Ed.*, 2022, **61**, e202212872.

13 C. J. T. de Grotthuss, *Ann. Chim.*, 1806, **58**, 54–74.

14 W. S. Tang, M. Matsuo, H. Wu, V. Stavila, W. Zhou, A. A. Talin, A. V. Soloninin, R. V. Skoryunov, O. A. Babanova, A. V. Skripov, A. Unemoto, S.-I. Orimo and T. J. Udovic, *Adv. Energy Mater.*, 2016, **6**, 1502237.

15 Z. Xu, Y. Lin, Y. Xia, Y. Jiang, X. Feng, Z. Liu, L. Shen, M. Zheng and Y. Xia, *J. Power Sources*, 2025, **637**, 236591.

16 S. Bureekaew, S. Horike, M. Higuchi, M. Mizuno, T. Kawamura, D. Tanaka, N. Yanai and S. Kitagawa, *Nat. Mater.*, 2009, **8**, 831–836.

17 S. Horike, D. Umeyama, M. Inukai, T. Itakura and S. Kitagawa, *J. Am. Chem. Soc.*, 2012, **134**, 7612–7615.

18 D. Umeyama, S. Horike, M. Inukai and S. Kitagawa, *J. Am. Chem. Soc.*, 2013, **135**, 11345–11350.

19 S. Horike, W. Chen, T. Itakura, M. Inukai, D. Umeyama, H. Asakura and S. Kitagawa, *Chem. Commun.*, 2014, **50**, 10241–10243.

20 N. Ma, S. Kosasang, A. Yoshida and S. Horike, *Chem. Sci.*, 2021, **12**, 5818–5824.

21 M. Mizuno, A. Iwasaki, T. Umiyama, R. Ohashi and T. Ida, *Macromolecules*, 2014, **47**, 7469–7476.

22 M. Mizuno, M. Chizuwa, T. Umiyama, Y. Kumagai, T. Miyatou, R. Ohashi, T. Ida, M. Tansho and T. Shimizu, *Hyperfine Interact.*, 2015, **230**, 95–100.

23 M. Mizuno, T. Narita, R. Une, R. Ohashi and T. Ida, *Chem. Lett.*, 2018, **47**, 411–413.

24 H. Zhu, X. Wang, R. Vijayaraghava, Y. Zhou, D. R. MacFarlane and M. Forsyth, *J. Phys. Chem. Lett.*, 2018, **9**, 3904–3909.

25 A. Mondal and S. Balasubramanian, *J. Phys. Chem. C*, 2016, **120**, 22903–22909.

26 G. Kim, F. Blanc, Y.-Y. Hu and C. P. Grey, *J. Phys. Chem. C*, 2013, **117**, 6504–6515.

27 R. M. P. Colodrero, P. Olivera-Pastor, A. Cabeza and M. Bazaga-García, *Materials*, 2022, **15**, 1292.

28 R. H. Blessing and E. L. McGandy, *J. Am. Chem. Soc.*, 1972, **94**, 4034–4035.

29 R. H. Blessing, *Acta Crystallogr., Sect. B: Struct. Sci.*, 1986, **42**, 613–621.

30 Q. Xia, X. Jiang, L. Qi, C. Wu, Z. Lin, Z. Huang, M. G. Humphrey, K. Tatsumi and C. Zhang, *Inorg. Chem. Front.*, 2024, **11**, 8813–8823.

31 J. M. Taylor, S. Dekura, R. Ikeda and H. Kitagawa, *Chem. Mater.*, 2015, **27**, 2286–2289.

32 J. Lee, D.-W. Lim, S. Dekura, H. Kitagawa and W. Choe, *ACS Appl. Mater. Interfaces*, 2019, **11**, 12639–12646.

33 Y. Miyazaki, R. Nakayama, N. Yasuo, Y. Watanabe, R. Shimizu, D. M. Packwood, K. Nishio, Y. Ando, M. Sekijima and T. Hitosugi, *AIP Adv.*, 2020, **10**, 045231.

34 L. Navarrete, A. Andrio, S. Escolástico, S. Moya, V. Compañ and J. M. Serra, *Membranes*, 2019, **9**, 49.

35 T. Umiyama, R. Ohashi, T. Ida and M. Mizuno, *Chem. Lett.*, 2013, **42**, 1323–1325.

36 (*a*) CCDC 2476711: Experimental Crystal Structure Determination, 2025, DOI: **10.5517/ccdc.csd.cc2p46xz**; (*b*) CCDC 2476720: Experimental Crystal Structure Determination, 2025, DOI: **10.5517/ccdc.csd.cc2p4769**.